Relevance of the Drying Step in the Preparation by Impregnation of Zn/SiO_2 Supported Catalysts

Cyril Chouillet,[†,||] Françoise Villain,[‡,§] Maggy Kermarec,[†] Hélène Lauron-Pernot,[†] and Catherine Louis*[,†]

Laboratoire de Réactivité de Surface, UMR 7609 CNRS, and Laboratoire de Chimie Inorganique et Matériaux Moléculaires, UMR 7071 CNRS, Université Pierre et Marie Curie, 4 place Jussieu, F75252 Paris Cedex 05, France, and Laboratoire pour l'Utilisation du Rayonnement Electromagnétique, Bâtiment 209D, Centre Universitaire, B.P. 34, 91898 Orsay Cedex, France

Received: November 25, 2002

Zinc supported over silica materials, which are widely used in heterogeneous catalysis, are prepared in most cases by incipient wetness impregnation with solutions of zinc nitrate. After calcination, the formation of ZnO is usually assumed, although not always fully demonstrated. The goal of this paper is to clarify the nature of the zinc phase present in Zn/SiO_2 samples not only after calcination, but also after drying. To achieve this goal, the supported zinc phase was characterized in such systems after drying (between 25 and 200 °C) and after calcination (450 °C). The use of four complementary techniques, UV−visible, diffuse reflectance infrared, and X-ray absorption spectroscopies and X-ray diffraction, allowed us to show that the ZnO phase supposed to be formed during calcination is a minor phase and that the main phase is a poorly crystallized zinc silicate $Zn_4Si_2O_7(OH)_2 \cdot H_2O$, also called hemimorphite. ZnO formation strongly depends on the drying temperature after impregnation: after drying at 25, 50, and 200 °C, ZnO does not form after calcination. After drying at 25 or 50 °C, the supported zinc phase is an amorphous nitrate, whereas after drying at 200 °C, it is almost already fully transformed into zinc silicate. At intermediate drying temperatures between 90 and 150 °C, part of the zinc forms crystallized zinc hydroxynitrates, which lead to the ZnO phase after calcination; almost all of the remaining zinc is a zinc silicate.

Introduction

Silica-supported zinc materials have demonstrated their efficiency as catalysts in many reactions. For example, they behave efficiently in the addition of primary alcohols to alkynes and allenes,[1] in the photooxidation of propene to propene oxide,[2] in the Beckmann rearrangement of cyclohexanone oxime,[3] and in the dehydrogenation of methanol to formaldehyde.[4] They have also been studied in the water−gas shift reaction[5] and in the formation of acrylaldehyde by aldol condensation.[6] On the other hand, zinc associated with copper supported on silica is efficient in catalyzing the hydrogenolysis of esters[7,8] and the dehydrogenation of alcohols.[9] In addition, zinc supported on silica, in the presence, or lack thereof, of copper, has been extensively used as a model catalyst for the synthesis of methanol.[10,11]

Usually, silica-supported zinc catalysts are prepared by the impregnation of silica with a solution of a nitrate, acetate, or chloride precursor salt. In catalytic studies, it is commonly claimed that ZnO is obtained after drying and calcination.[5,6,12] When ZnO is not observed in the XRD pattern[13] or when the UV−visible spectrum gives an absorption at a wavelength lower than 250 nm,[2] i.e., lower than that of the band gap of ZnO at 350 nm, the formation of ZnO is nevertheless assumed in most studies, but as a well-dispersed ZnO phase. Other authors postulate the occurrence of a strong interaction between zinc and silica[3,4,14] to explain the peculiar properties of their materials: unexpected reactivity, formation of new acidic sites or different optical properties. Characterization by ion scattering spectroscopy[15] of calcined Zn/SiO_2 prepared by impregnation with zinc nitrate indicates that the zinc phase appears similar to β-Zn_2SiO_4. Finally, Breuer et al.,[1] who studied zinc nitrate or zinc acetate catalysts supported on silica in the reaction of addition of methanol to 2-methoxypropene, showed that the EXAFS signal of the active catalyst is similar to that of a zinc silicate. They could not discriminate between the different types of zinc silicates, i.e., zinc orthosilicate (Zn_2SiO_4), hemimorphite [$Zn_4Si_2O_7(OH)_2 \cdot H_2O$], and sauconite or zinc phyllosilicate [$Zn_3Si_4(OH)_2 \cdot 4H_2O$]. However, they showed that bulk hemimorphite is as active and selective as the amorphous phase obtained from the zinc salt deposited on silica.

It must be recalled that the nature of a supported phase depends on the method of preparation, the nature of the precursors, and the conditions of activation. For instance, previous works performed by our group showed that a silica support can act as a chemical reagent and form a supported silicate phase, such as phyllosilicates in the case of the preparation of Ni/SiO_2,[16−18] Cu/SiO_2,[19] and Co/SiO_2.[20] In the case of Zn/SiO_2, the identification of these surface compounds is still a matter of discussion, as reported above. Moreover, the influence of the synthesis conditions has not been investigated. In a former study on the Cu/SiO_2 system,[21] our group also demonstrated the relevance of the drying conditions after

* To whom correspondence should be addressed. E-mail: louisc@ccr.jussieu.fr.

† Laboratoire de Réactivité de Surface, UMR 7609 CNRS, Université Pierre et Marie Curie.

‡ Laboratoire de Chimie Inorganique et Matériaux Moléculaires, UMR 7071 CNRS, Université Pierre et Marie Curie.

§ LURE.

|| Deceased at the age of 25 during his period in the laboratory. This work is dedicated to him.

10.1021/jp022481+ CCC: $25.00
Published on Web 03/26/2003

impregnation. When the samples were dried at 25 °C, they gave rise to small particles after reduction because the amorphous phase of copper nitrate was widely spread onto the silica surface. In contrast, when the samples were dried in air at 100 °C, copper nitrate gradually transformed into large particles of copper hydroxynitrate and into large metal particles after reduction. It is well-known that, like copper nitrate, zinc nitrate is able to transform into hydroxynitrates. Depending on the temperature, it can transform into three types of zinc hydroxynitrates, $Zn(OH)(NO_3)\cdot H_2O$, $Zn_3(OH)_4(NO_3)_2$, and $Zn_5(OH)_8(NO_3)_2\cdot 2H_2O$[22−24] whose formation can influence the final state of the catalyst.

The goal of this paper is to study the influence of the drying temperature of Zn/SiO_2 samples prepared by impregnation of silica with zinc nitrate on the final state of the material, i.e., on the nature and dispersion of the Zn^{II} species obtained after drying and also after calcination. The Zn/SiO_2 samples were characterized after drying and after calcination by X-ray diffraction; UV−visible spectroscopy, DRIFTS; and X-ray absorption spectroscopy (XAS), which has been especially useful in identifying amorphous zinc phase. Several zinc silicates were synthesized as references, according to the original deposition−precipitation method,[17,25] which was applied to the zinc−silica system[26] for the first time here.

I. Experimental Section

1. Sample Preparation. *a. Zn/SiO_2 Samples.* The samples were prepared with a nonporous silica (Aerosil Degussa 380, 380 $m^2\cdot g^{-1}$ according to the manufacturer). Samples containing 10 wt % of Zn were prepared by incipient wetness impregnation with zinc nitrate [$Zn(NO_3)_2\cdot 6H_2O$; 99.999%, Aldrich]. A 5.1-mL portion of an aqueous solution of zinc nitrate (0.9 $mol\cdot L^{-1}$) was added dropwise to 3 g of silica. The mixture was thoroughly hand-mixed for about 40 min until a gel was obtained. We chose the most common method of drying the catalysts, i.e., drying in a preheated oven and under static air. Special attention was paid to the drying conditions to obtain reproducible results under our experimental conditions. First, the gel was spread as a thin bed in the bottom of a Petri plate. The samples were dried in air at room temperature (RT) or for 24 h in a given oven (systematically the same one) previously heated at 50, 90, 120, 150, or 200 °C. After being dried, the samples were cooled in ambient air and stored in a desiccator under vacuum. The samples were calcined according to the following temperature profile: heat from RT to 450 °C at a heating rate of 7.5 $°C\cdot min^{-1}$ under a flow of industrial air (Air Liquide, 100 $mL\cdot min^{-1}$) and then hold at 450 °C for 3 h.

b. Zinc Hydroxynitrates. The preparations of the three zinc hydroxynitrates, $Zn(OH)(NO_3)\cdot H_2O$, $Zn_3(OH)_4(NO_3)_2$ and $Zn_5(OH)_8(NO_3)_2\cdot 2H_2O$, were performed according to the procedures reported by Louër et al.[22,23] and Stählin and Ostwald.[24]

$Zn(OH)(NO_3)\cdot H_2O$ was prepared as follows: $Zn(NO_3)_2\cdot 6H_2O$ was melted at 40 °C and then spread into the bottom of a Petri plate that was put in an oven at 65 °C for 2 weeks.[22]

The method of preparation of $Zn_3(OH)_4(NO_3)_2$ is the same as that of $Zn(OH)(NO_3)\cdot H_2O$, except that the sample was maintained in the oven at 120 °C for 7 days.[23]

$Zn_5(OH)_8(NO_3)_2\cdot 2H_2O$ was obtained from a mixture of aqueous solutions of zinc nitrate (2 M, 50 mL) and urea (2 M, 50 mL) that was stirred under bubbling N_2 and heated under reflux at 60 °C for 15 h. The solid was dried at RT after filtration.[24]

For the sake of brevity, these compounds are noted Zn_1, Zn_3, and Zn_5, respectively, in the following.

c. Zinc Silicates. Sauconite, $Si_4Zn_3O_{10}(OH)_2$, which is also called zinc phyllosilicate because it exhibits a talc-like layered structure (the layers consist of two sheets of linked SiO_4 units sandwiching the brucite-type sheets) was prepared according to the deposition−precipitation method, which was previously used for the preparation of nickel phyllosilicate[17] and which was applied for the first time here to the preparation of zinc phyllosilicate: According to this approach, 380 mg of silica was placed into a vessel thermostated at 90 °C; 50 mL of an aqueous solution containing zinc nitrate (1.411 g, $Zn/Si = 0.75$), urea (0.42 M), and nitric acid (0.02 M) was added; and the suspension was stirred magnetically for 4 days. Then, the suspension was centrifuged, and the sample was washed three times. After addition of 20 mL of distilled water, the mixture was stirred for 10 min at 50−60 °C before filtration. Finally, the sample was dried at 90 °C for 24 h.

Hemimorphite [$Zn_4Si_2O_7(OH)\cdot H_2O$] was obtained by hydrothermal treatment of the zinc phyllosilicate. For this synthesis, 200 mg of zinc phyllosilicate was placed into a Teflon autoclave containing 67 mL of water. The hydrothermal treatment was performed at 180 °C for 12 days.

Willemite (α-Zn_2SiO_4) was obtained by thermal treatment of hemimorphite at 800 °C for 1 h.

2. Characterization Techniques. X-ray diffraction (XRD) patterns were recorded on a Siemens diffractometer (D500) using the Cu Kα radiation. Phase identifications were performed by comparison with the tabulated Joint Committee on Powder Diffraction Standards (JCPDS) *d* spacing files.

Diffuse reflectance FTIR (DRIFT) spectra of the Zn/SiO_2 samples diluted in diamond (1:5 w/w) were recorded on a Bruker IFS 66 V spectrometer in the 3800−600 cm^{-1} range (resolution 4 cm^{-1}, 512 scans per spectrum). The samples were treated in situ for 2 h at 50 °C under a flow of argon (100 $mL\cdot min^{-1}$) to remove the physically adsorbed water. This temperature is below the drying temperature except for the 25 °C-dried sample. All of the DRIFT spectra were converted into Kubelka−Munk units after subtraction of the spectrum of diamond treated under the same conditions.

XAS (extended X-ray absorption) measurements were performed at the Zn K edge on the dried and calcined Zn/SiO_2 samples at the XAS 13 beam line of the DCI storage ring (operating with positrons at 1.85 eV and a mean ring current of 300 mA) of the LURE synchrotron radiation facility (Orsay, France). The samples were diluted with cellulose and pressed as pellets. The EXAFS (extended X-ray absorption fine structure) spectra were recorded at 77 K, and the XANES (X-ray absorption near edge structure) spectra at RT, in the transmission mode using two argon-filled ionization chambers. For the XANES measurements, a double-crystal Si(311) monochromator was used, and the energies were scanned in 0.4 eV steps from 9640 to 9770 eV. For the EXAFS measurements, a channel-cut Si(111) monochromator was used, and the energies were scanned in 2 eV steps from 9550 to 10 550 eV. The energy was calibrated using a Zn metal foil reference. For each sample, the XANES spectra were recorded two times, and the EXAFS spectra, three times. The XAS spectra of an aqueous solution of zinc nitrate $[Zn(H_2O)_6]^{2+}$, the three zinc hydroxynitrates, the three zinc silicates, and ZnO (Aldrich) were also recorded as references. After background correction, the XANES spectra were normalized in the middle of the first EXAFS oscillation. For EXAFS analyses, it will be shown in Results section II.3.c that multiple scattering is negligible in the 0−4.5 Å distance range. Thus, the EXAFS analyses were performed in the framework of single-scattering treatments with the package of

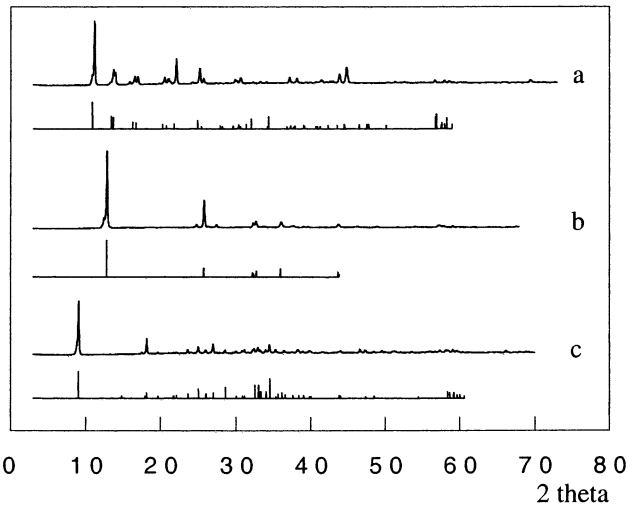

Figure 1. XRD patterns of the three synthesized zinc hydroxynitrates and comparison to their JCDS files: (a) $Zn(OH)(NO_3)\cdot H_2O$ and JCPDS file 84-1907, (b) $Zn_3(OH)_4(NO_3)_2$ and JCPDS file 70-1361, (c) $Zn_5(OH)_8(NO_3)_2\cdot 2H_2O$ and JCPDS file 24-1460.

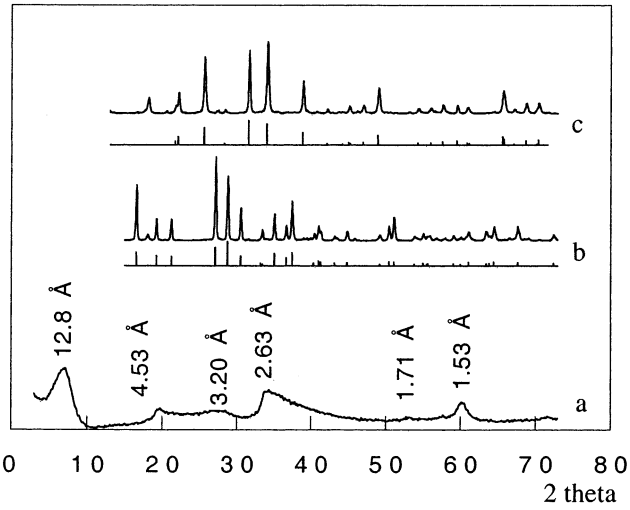

Figure 2. XRD patterns of the three synthesized zinc silicates and comparison to their JCDS files: (a) zinc phyllosilicate [$Zn_3Si_4O_{10}(OH)_2$], (b) hemimorphite [$Zn_4Si_2O_7(OH)\cdot H_2O$] and JCPDS file 5-555, (c) willemite (α-Zn_2SiO_4) and JCPDS file 37-1485.

programs "EXAFS pour le Mac".[27] The $k\chi(k)$ functions were extracted from the data following the procedure proposed by Lengeler and Eisenberger[28] using a linear preedge background and a combination of polynomials and spline atomic absorption background. The Fourier transforms (FT) were calculated on $w(k)k^3\chi(k)$, where $w(k)$ is a Kaiser−Bessel window with a smoothness parameter equal to 3. The k limits are 2.1 and 15 $Å^{-1}$. It should be noted that the FT's are presented without phase correction in the figures. Single-scattering fits of experimental curves were performed with the Round Midnight program.[29] Ab initio amplitude and phase functions $|f_i(k,R_i)|$ and $|\phi_i(k,R_i)|$ were calculated using FEFF7 code[30] for hemimorphite and hexaquozinc nitrate structures with an amplitude reduction factor S_0^2 fixed to 1 and a global Debye−Waller factor equal to 0.07 Å. The calculations were performed with single-scattering paths only ($N_{leg} = 2$) and multiple-scattering paths ($N_{leg} = 8$) to check the importance of multiple scattering.

UV−visible spectra (200−500 nm) of the calcined Zn/SiO_2 samples were collected on a Cary 5E spectrophotometer equipped with a Cary4/5 diffuse reflection sphere. The baseline was recorded using a poly(tetrafluoroethylene) reference.

The sizes of the zinc oxide particles obtained after calcination of the Zn/SiO_2 samples were measured from the electron micrographs obtained by transmission electron microscopy (TEM, JEOL 100 CXII). The average particle diameter was deduced from the equation

$$d_m = \Sigma n_i d_i / \Sigma n_i$$

where n_i is the number of particles of diameter d_i. The detection limit of the particles is ∼10 Å.

II. Results

1. Characterization of the Zinc References. *a. Zinc Hydroxynitrates.* The XRD diffractograms in Figure 1 show that the various syntheses of zinc hydroxynitrates Zn_1, Zn_3, and Zn_5 were successful. Indeed, they fit with their respective JCDS files.

b. Zinc Silicates. Zinc phyllosilicate or sauconite (Figure 2a) exhibits an XRD pattern characteristic of a poorly crystallized compound with a lamellar structure of montmorillonite type, with *hk* and *00l* lines. Natural sauconites, and also synthesized ones, exhibit low crystallinity,[31,32] so the indexation was performed on the basis of the XRD patterns of other phyllosilicates, such as nickel phyllosilicate.[17,33,34] Hence, the diffraction peaks can be attributed as follows: 12.8 Å is the (001) line of the basal spacing; 4.53 Å, the (02−11) line; 3.2 Å, the (003) line; 2.63 Å, the (201) and (13−20) lines; 1.71 Å, the (15−24−31) lines and 1.53 Å, the (06−33) lines.

The two other zinc silicates correspond to the expected structure as their XRD patterns fit with their respective JCPDS files (Figure 2b,c).

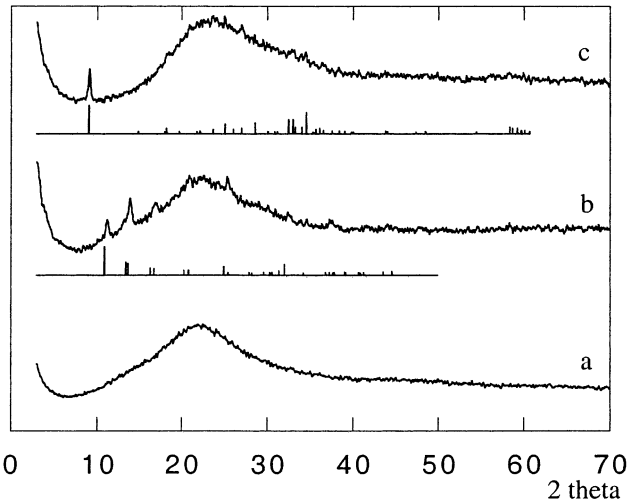

Figure 3. XRD patterns of the Zn/SiO_2 samples dried at (a) 25 °C (the same diffractogram was obtained at 50 and 200 °C), (b) 90 °C (the same diffractogram was obtained at 120 °C) and the JCPDS file 84-1907 of Zn_1, (c) 150 °C and JCPDS file 24-1460 of Zn_5.

2. Characterization of the Dried Zn/SiO_2 Samples. *a. XRD.* The XRD patterns of the Zn/SiO_2 samples show that the zinc supported phase is amorphous when the samples are dried at RT and 50 and 200 °C (Figure 3a). In contrast, those dried at 90, 120, and 150 °C exhibit weak lines superimposed onto the broad contribution of the amorphous silica (Figure 3b,c). Comparisons with the JCPDS files or the XRD patterns of the three zinc hydroxynitrates (Figure 1) indicate that these weak lines can be attributed to two types of zinc hydroxynitrates (i) Zn_1 in the samples dried at 90 and 120 °C (Figure 3b), with characteristic lines at $2\theta = 10.9$, 13.7, and 16.5°, and (ii) Zn_5 in

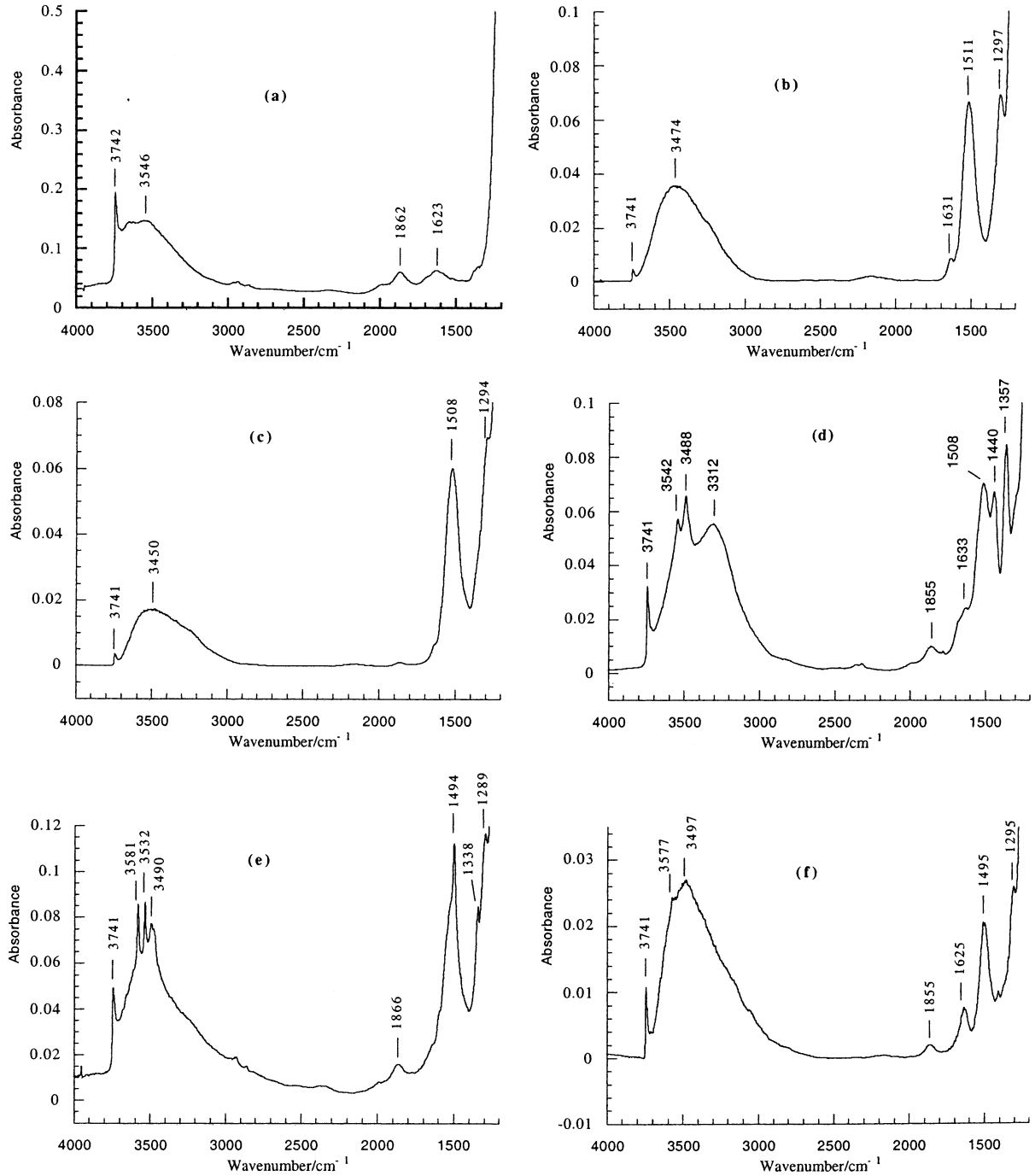

Figure 4. DRIFT spectra of (a) silica and the Zn/SiO_2 samples dried at (b) 25, (c) 50, (d) 120, (e) 150, (f) 200 °C.

the sample dried at 150 °C (Figure 3c), with the main (100) line at $2\theta = 9°$.

b. DRIFT. The DRIFT spectra of the Zn/SiO_2 samples also depend on the drying temperature (Figure 4). The DRIFT spectra of the three reference hydroxynitrates Zn_1, Zn_3, and Zn_5, which have been already reported and discussed,[35] are displayed in Figure 5 for samples subjected to the same pretreatment at 50 °C for 2 h. It must be kept in mind that, under such conditions, Zn_5 loses its water molecules and shows a spectrum characteristic of $Zn_5(OH)_8(NO_3)_2$.[35] The characteristic bands of Zn_1, Zn_3, and Zn_5 are observed between 3600 and 3300 cm^{-1}, i.e., in the range of the stretching mode of OH vibrations (ν_{OH}), and between 1550 and 1290 cm^{-1}, i.e., in the range of the stretching mode of the nitrate vibrations (ν_{NO_3}). From these spectra, it can be anticipated that the presence of Zn_3 on silica is not easily detectable because (i) in the nitrate vibration range, it is very difficult to discriminate the ν_{NO_3} bands of Zn_3 and Zn_5 (Figure 5b,c), and (ii) in the OH vibration range, the ν_{OH} band of silica, whose DRIFT spectrum is reported in Figure 4a, might hide that of Zn_3.

The spectra of the Zn/SiO_2 samples dried at 25 and 50 °C (Figure 4b,c) do not show vibration bands characteristic of the presence of zinc hydroxynitrates in the ν_{OH} region. In addition to the bands of silica (Figure 4a), they exhibit two strong ν_{NO_3} bands at ~1510 and ~1295 cm^{-1} which cannot be attributed to zinc hydroxynitrates either. They arise from the splitting of the E′ stretching mode (ν_3) of nitrate ion at 1390 cm^{-1} present in nitrate compounds such as zinc nitrate.[36,37] Such a splitting is characteristic of coordinated nitrate ions and results from the lowering of the D_{3h} symmetry of the NO_3^- free anion. In the

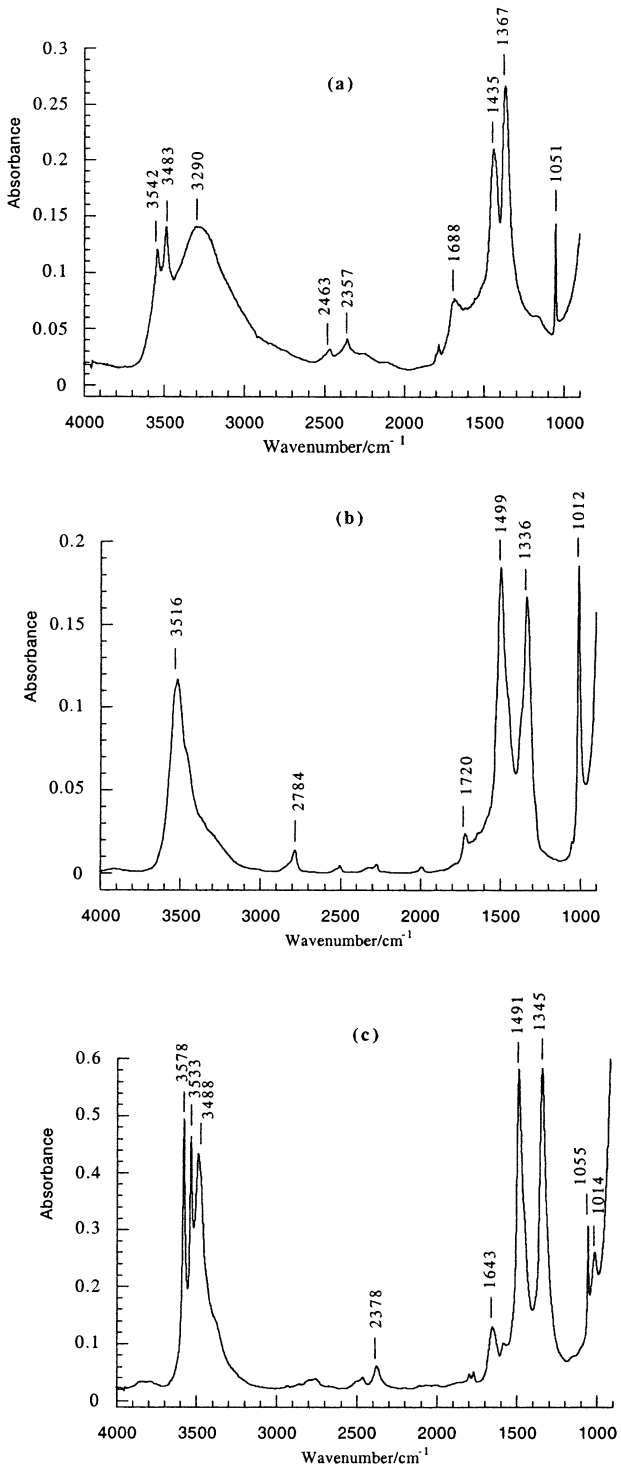

Figure 5. DRIFT spectra of zinc hydroxynitrates (a) $Zn(OH)(NO_3)\cdot H_2O$, (b) $Zn_3(OH)_4(NO_3)_2$, (c) $Zn_5(OH)_8(NO_3)_2\cdot 2H_2O$.

present case, the splitting might be due to the presence of silica. In the spectrum of the sample dried at 120 °C (Figure 4d), the ν_{OH} bands at 3542 and 3488 cm^{-1} and the ν_{NO_3} bands at 1440 and 1357 cm^{-1} are characteristic of the presence of the Zn_1 species (Figure 5a). In the spectrum of the sample dried at 150 °C (Figure 4e), the ν_{OH} bands at 3581, 3532, and 3490 cm^{-1} and the ν_{NO_3} bands at 1494 and 1338 cm^{-1} are characteristic of the presence of the Zn_5 species (Figure 5c). In both of these spectra, additional bands of nitrate are present at 1510 and 1295 cm^{-1}, which indicates that zinc nitrate is still present in these samples. In the spectrum of the sample dried at 200 °C (Figure 4f), the ν_{NO_3} bands of the hydroxynitrate species are much smaller. Only, a residual ν_{NO_3} band at 1495 cm^{-1} remains, as well as a shoulder at 1295 cm^{-1}. These signals can be attributed to traces of either Zn_5 or of Zn_3 and to traces of nitrate. The resolution of the spectrum in the ν_{OH} range does not permit the discrimination between the two hydroxynitrates.

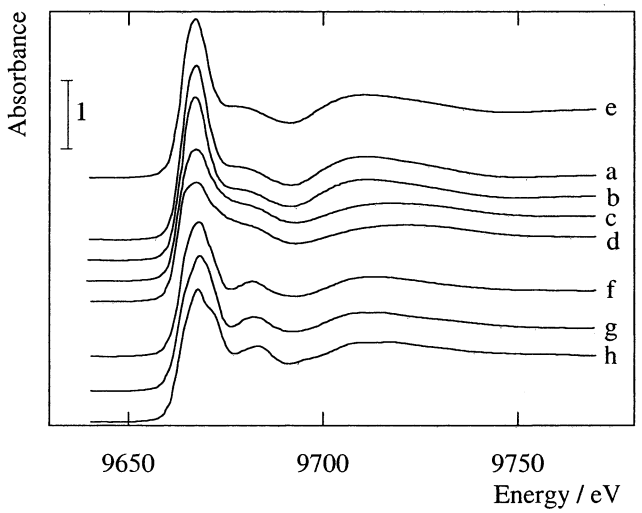

Figure 6. XANES spectra of the Zn/SiO_2 samples dried at (a) 25, (b) 50, (c) 120, (d) 200 °C, and reference (e) $Zn(NO_3)_2$ in solution, (f) $Zn(OH)(NO_3)\cdot H_2O$, (g) $Zn_3(OH)_4(NO_3)_2$, (h) $Zn_5(OH)_8(NO_3)_2\cdot 2H_2O$.

It should be noted that the spectra of the reference zinc silicates were also recorded. However, they are not reported in this paper because their characteristic bands were observed below 1200 cm^{-1}, i.e., in the range of absorption of silica (Figure 4a). Identification of supported zinc silicates is not possible using this technique.

c. XAS. The samples dried at 25, 50, 120, and 200 °C were also studied by XAS. The XANES spectra of the 25 and 50 °C-dried samples (Figure 6a,b) are similar to each other and to that of $[Zn(H_2O)_6]^{2+}$ (zinc nitrate in aqueous solution) (Figure 6e). They are characteristic of a regular octahedral symmetry and the $3d^{10}$ configuration of Zn^{2+}: a single intense band of the edge and absence of preedge. Moreover, the same first EXAFS oscillation is observed with these two samples and $[Zn(H_2O)_6]^{2+}$. This indicates the same Zn first-neighbor distance.

In contrast, the XANES spectra of the 120 and 200 °C-dried samples (Figure 6c,d) show a broader and much less intense edge that can be attributed to a lowering of the O_h symmetry of Zn^{II}. The shift of the first EXAFS oscillation to higher energy and its lower intensity indicate both a shortening of the Zn first-neighbor distance and a smaller number of neighbors. It must be noted that the XANES spectra of the dried samples are different from those of the three hydroxynitrates shown in Figure 6f,g.

The EXAFS analysis confirms these features. The moduli of the Fourier transforms of the EXAFS signals of the 25 and 50 °C-dried samples (Figure 7a,b) are identical and show a single peak (~1.67 Å) as in the case of $[Zn(H_2O)_6]^{2+}$ (Figure 7e). The difference in intensity is due to the fact that the spectrum of $[Zn(H_2O)_6]^{2+}$ was recorded at room temperature. In contrast, the moduli of the Fourier transforms of the EXAFS signals of the 120 and 200 °C-dried samples are different (Figure 7c,d). The first peak is much less intense and shifted toward shorter distances, and a second peak of low intensity is visible at ~2.7 Å. This indicates that a new zinc species forms at these temperatures of drying. The Fourier transforms of the EXAFS signals of the zinc hydroxynitrates (Zn_1 and Zn_5) also exhibit

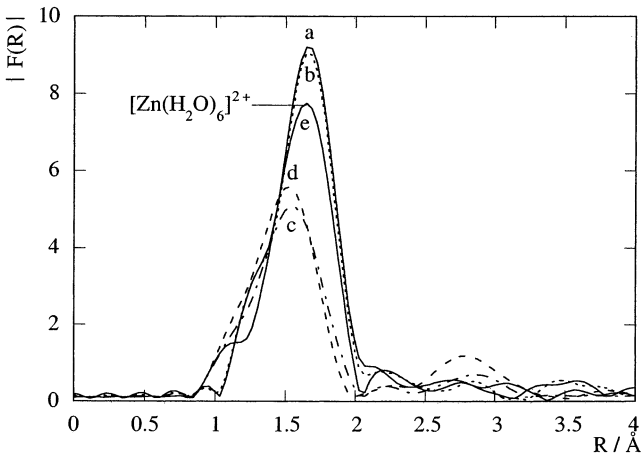

Figure 7. Fourier transforms of the EXAFS spectra of the Zn/SiO_2 samples dried at (a) 25, (b) 50, (c) 120, (d) 200 °C, and reference (e) $Zn(NO_3)_2$ in solution.

TABLE 1: Best Parameters[a] for the Fit of the EXAFS Spectra of the Dried Zn/SiO_2 Samples and of the Solution of Zinc Nitrate

sample	backscatterer	N	σ (Å)	R (Å)	ΔE_0 (eV)	ρ (%)
25°C-dried Zn/SiO_2	O	6	0.08	2.09	−0.5	1.6
50 °C-dried Zn/SiO_2	O	6	0.08	2.09	−1.0	2.0
120 °C-dried Zn/SiO_2	O	4.4	0.10	2.01	−2.0	
	Si	0.5	0.11	3.12	−2.0	1.7
	Zn	0.9	0.11	3.31	−7.0	
200 °C-dried Zn/SiO_2	O	4.1	0.09	1.98	−2.5	
	Si	0.8	0.10	3.12	−2.0	3.0
	Zn	1.1	0.10	3.31	−7.0	
$[Zn(H_2O)_6]^{2+}$	O	6	0.09	2.08	−2.0	2.8

[a] N = number of neighbors, σ (Å) = Debye−Waller factor, R (Å) = distance between Zn and a backscatterer, ΔE_0 (eV) = energy shift; ρ (%) = agreement factor.

several peaks, but neither the moduli nor the imaginary parts fit with those of the EXAFS signals of the 120 and 200 °C-dried samples (figure not shown). Hence, the main zinc species in these samples dried at 120 and 200 °C is not a zinc hydroxynitrate.

The fit parameters obtained within the framework of a single-scattering analysis are reported in Table 1. For the 25 and 50 °C-dried samples, the first and only shell contribution filtered in the range 0.80−2.10 Å fits with six oxygen atoms at 2.09 Å. Table 1 also shows that this result is fully consistent with the hypothesis of the presence of $[Zn(H_2O)_6]^{2+}$ as in zinc nitrate.

For the 120 and 200 °C-dried samples, the first-shell contributions filtered in the range 0.80−2.10 Å fit with 4.4 and 4.1 oxygen atoms at 2.01 and 1.98 Å, respectively, and indicate the presence of Zn^{II} in 4-fold coordination. This result is in agreement with the XANES data. On the other hand, the shape of the second-shell contributions filtered in the range 2.10−3.50 Å indicates the presence of heavy backscatterers. For the 120 °C-dried sample, the best fit was obtained with 0.5 silicon atoms at 3.12 Å and 0.9 zinc atoms at 3.31 Å. For the 200 °C-dried sample, the best fit was obtained with the same distances but with higher numbers of silicon and zinc atoms, 0.8 and 1.1, respectively. In the Discussion section, it will be shown that the main species in these samples is a poorly crystallized zinc silicate of hemimorphite type.

3. Characterization of the Calcined Zn/SiO_2 Samples. *a. XRD.* After calcination, the samples that were dried at 120 and 150 °C exhibit diffraction lines characteristic of ZnO (Figure 8), in contrast with the 25, 90, and 200 °C-dried samples, which do not show any diffraction lines after calcination. The diffraction lines of the 120 °C-dried sample are much weaker than those of the 150 °C-dried sample. To evaluate the amount of ZnO in the samples, the intensities of the diffraction patterns are compared to those of various mechanical mixtures of silica and commercial ZnO, i.e., of well-crystallized ZnO (Figure 8c). One can deduce that about 10% of the Zn phase in the calcined 150 °C-dried sample is ZnO. However, the calcined Zn/SiO_2 samples might also contain poorly crystallized ZnO or ZnO particles too small to be detected by XRD.

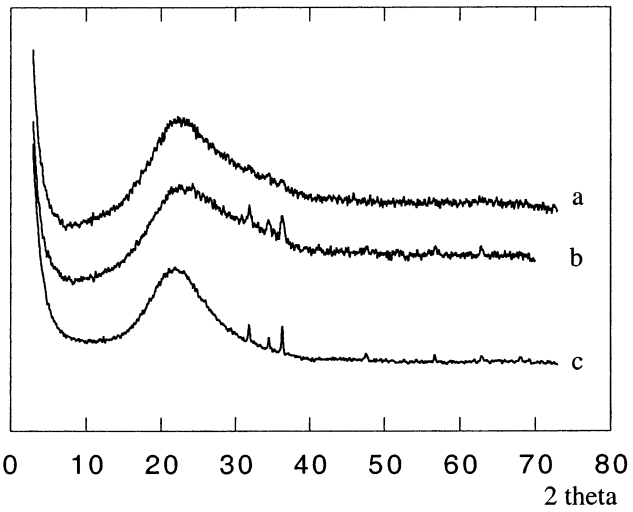

Figure 8. XRD patterns of Zn/SiO_2 samples calcined at 450 °C after drying at (a) 120 °C, (b) 150 °C, and of (c) a mechanical mixture of commercial ZnO and silica (1% ZnO in silica, i.e., 0.8% of Zn in silica).

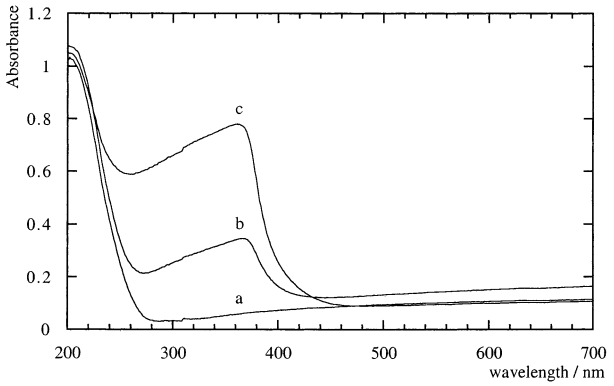

Figure 9. UV−visible spectra of Zn/SiO_2 samples calcined at 450 °C after drying at (a) 25, (b) 90, (c) 150 °C.

b. UV−Visible Spectroscopy. In contrast to the UV−visible spectrum of the calcined 25 °C-dried sample (Figure 9a), the UV−visible spectra of the calcined 120 and 150 °C-dried samples exhibit an absorption band with a maximum at 370 nm and a threshold at 400 nm (Figure 9c), as does the spectrum of the sample previously dried at 90 °C (Figure 9b). This absorption band is characteristic of ZnO, which is a semiconductor with a band gap of 3.35 eV.[38]

c. XAS. The XANES spectra of the calcined samples are all similar (Figure 10). In addition, it should be noted that they look more similar to those of willemite or hemimorphite (Figure 10c,d) than to those of zinc phyllosilicate or ZnO (Figure 10e,f). This first result indicates that the main zinc species present is not ZnO, even in the Zn/SiO_2 samples in which ZnO was detected by XRD, i.e., the calcined 120 and 150 °C-dried samples (Figure 8).

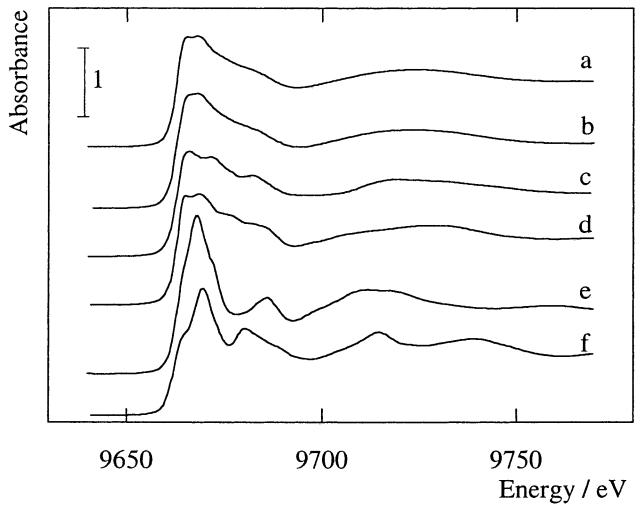

Figure 10. XANES spectra of the calcined Zn/SiO_2 samples: (a) 25 °C-dried, (b) 150 °C-dried, (c) willemite (α-Zn_2SiO_4), (d) hemimorphite [$Zn_4Si_2O_7(OH)\cdot H_2O$], (e) zinc phyllosilicate, (f) ZnO.

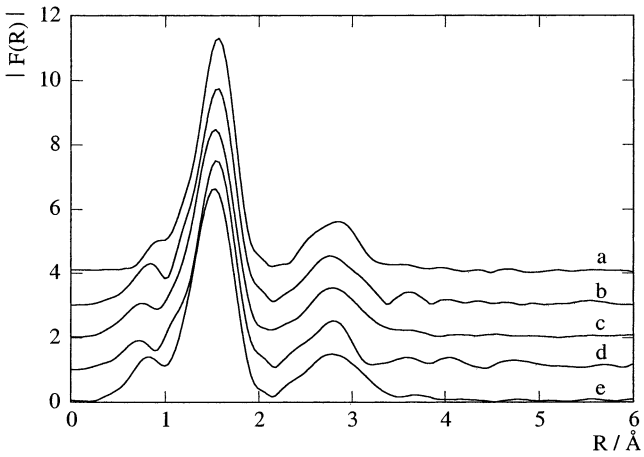

Figure 11. Fourier transforms of the EXAFS spectra of the calcined Zn/SiO_2 samples previously dried at (a) 25, (b) 50, (c) 120, (d) 150, (e) 200 °C-dried.

The moduli of the Fourier transforms of all of the EXAFS signals of the calcined samples show two main peaks at 1.56 and 2.80 Å (Figure 11). Before the analysis of these signals, the importance of multiple scattering was checked. FEFF calculations of the Fourier transforms of the EXAFS signals of hemimorphite and willemite were performed within the approximations of single scattering (SS) and multiple scattering (MS) from the known crystal structures of these two compounds. Figure 12 shows that multiple scattering is negligible up to 4.5 Å, which corresponds to a distance larger than that of Zn and/or Si second neighbors. Hence, fits can be carried out within the approximation of a single-scattering model if zinc silicate is the main species.

Quantitative analysis of all of the calcined samples shows that the first-shell contribution filtered between 0.80 and 2.10 Å fits with four oxygen atoms at 1.96 Å (Table 2). The second-shell contribution filtered in the range 2.10−3.50 Å can be fitted with heavier backscatterers, Si and Zn, as in the case of the three zinc silicates (Table 2). The results of the fits performed between 0.80 and 3.50 Å (Table 2, figures not shown) confirm that the main Zn species is not ZnO. Nor is it an isolated Zn^{II} species grafted onto the silica surface via Si−O−Zn bonds because the fits indicate the presence of Zn atoms as second neighbors. Hence, the Zn phase present in the calcined samples

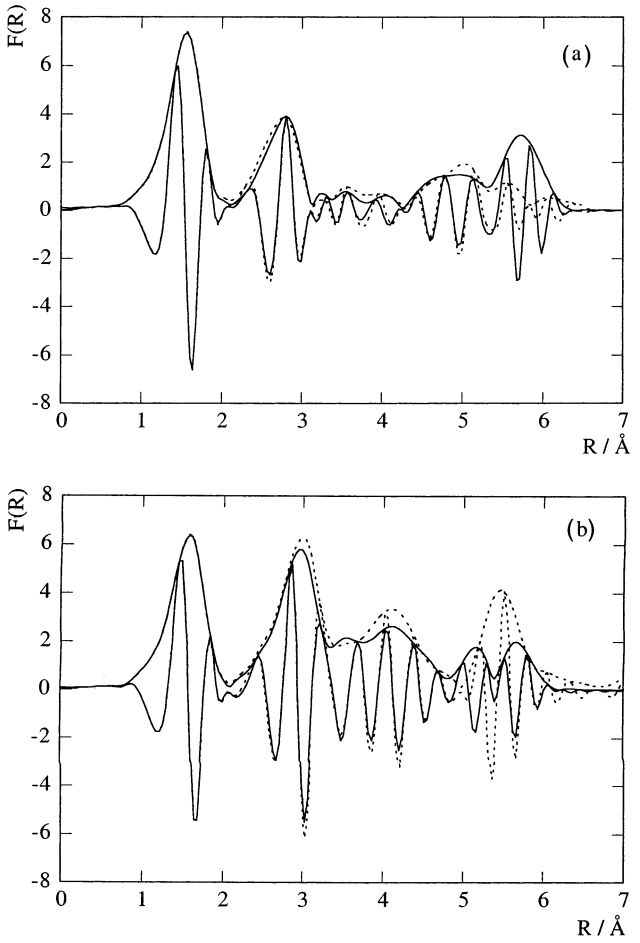

Figure 12. Comparison of the Fourier transforms calculated with FEFF for (a) hemimorphite and (b) willemite using single- (dotted lines) and multiple- (solid lines) scattering paths.

is probably a zinc silicate. The four oxygen atoms at a short distance (1.96 Å) indicates that this is not zinc phyllosilicate because Zn^{II} in this compound has O_h symmetry (six oxygen atoms at 2.08 Å from Zn^{II}). On the other hand, the Zn−Zn and Zn−Si mean distances are closer to those of hemimorphite than to those of willemite (Table 2). Moreover, the comparison of the imaginary part of the Fourier transform of the calcined 200 °C-dried sample, for instance, to that of willemite and hemimorphite shows that the Zn phase appears much more similar to hemimorphite (Figure 13a) than to willemite (Figure 13b). Hence, one can propose that the supported Zn phase is a zinc silicate of hemimorphite type.

It should be noted that the numbers of neighbors of Si (0.5−1) and Zn (1.4) atoms are smaller than those of reference hemimorphite (3 Si and 4 Zn) and that the Si/Zn atom ratio is lower than that of reference hemimorphite (Table 2). This is probably because supported hemimorphite is amorphous, which induces a local disorder. Such an observation has already been reported by Carriat et al.[39] in their study of the EXAFS signals of poorly and well-crystallized nickel phyllosilicates. In addition, because the theoretical Si EXAFS signal is weak compared to that of Zn and the number of neighbors and the Debye−Waller factor are strongly correlated, the absolute values given in Table 2 must be taken with caution.

It should be noted that the best fit of the EXAFS signal of the calcined 150 °C-dried sample gives significantly different results for the second shell than the other samples (Table 2): the Zn−Zn distance is shorter (3.27 instead of 3.31 Å) and the

TABLE 2: Best Parameters[a] for the Fit of the EXAFS Spectra of the Calcined Zn/SiO_2 Samples and of Reference Samples

sample	backscatterer	N	σ (Å)	R (Å)	ΔE_0 (eV)	ρ (%)
calcined	O	4.0	0.07	1.96	−1.5	
25°C-dried Zn/SiO_2	Si	1.0	0.09	3.12	−2.0	0.9
	Zn	1.4	0.10	3.31	−6.0	
calcined	O	4.0	0.08	1.96	−2.0	
50 °C-dried Zn/SiO_2	Si	1.0	0.09	3.12	−2.0	1.6
	Zn	1.4	0.11	3.31	−7.0	
calcined	O	4.0	0.08	1.96	−2.0	
120 °C-dried Zn/SiO_2	Si	0.9	0.08	3.12	−1.0	1.6
	Zn	1.4	0.10	3.31	−7.0	
calcined	O	4.0	0.08	1.96	−3.0	
150 °C-dried Zn/SiO_2	Si	0.5	0.09	3.12	−2.0	1.5
	Zn	1.4	0.10	3.27	−8.0	
calcined	O	4.0	0.08	1.96	−2.5	
200 °C-dried Zn/SiO_2	Si	0.9	0.09	3.12	−2.0	1.7
	Zn	1.4	0.11	3.31	−6.0	
ZnO[b]	O	4.0	0.06	1.98	−1.7	3.9
	Zn	12.0	0.07	3.23	−5.1	
hemimorphite[b]	O	4.0	0.06	1.96	0	
$Zn_4Si_2O_7(OH)_2 \cdot H_2O$	Si	3.0	0.09	3.12	0	3.0
	Zn	2.0	0.08	3.31	0	
	Zn	2.0	0.08	3.45	0	
willemite[b]	O	4.0	0.07	1.95	1.0	
α-Zn_2SiO_4	Si	4.0	0.13	3.18	−5.0	2.0
	Zn	4.0	0.11	3.20	−4.0	
zinc phyllosilicate[b]	O	6.0	0.075	2.08	−1.0	
$Zn_3Si_4(OH)_2 \cdot 4H_2O$	Zn	6.0	0.075	3.09	−5.0	2.5
	Si	4.0	0.075	3.27	−5.0	

[a] N = number of neighbors, σ (Å) = Debye−Waller factor, R (Å) = distance between Zn and a backscatterer, ΔE_0 (eV) = energy shift; ρ (%) = agreement factor. [b] N and R are in agreement with the crystallographic data of refs 40−43, respectively.

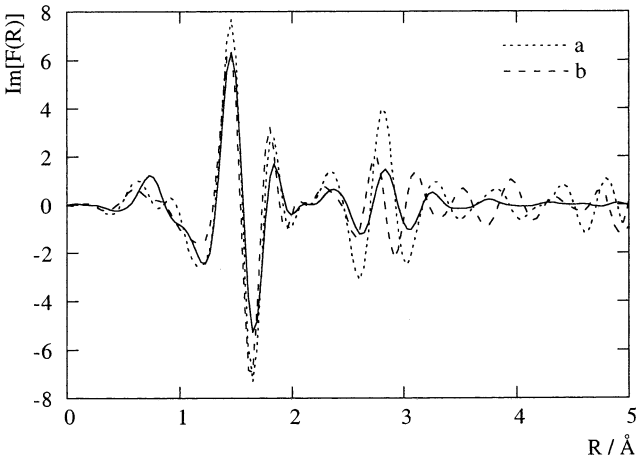

Figure 13. Comparison of the imaginary part of the Fourier transforms of the calcined 200 °C-dried sample (solid line) with those of (a) hemimorphite, (b) willemite (dotted lines).

number of Si neighbors and the Si/Zn ratio are smaller (0.5 Si instead of 0.9). These differences can be due to the presence of the small amount of ZnO detected by XRD.

The XAS results lead to the conclusion that all of the calcined Zn/SiO_2 samples contain a poorly crystallized zinc silicate phase of hemimorphite type. ZnO which was detected by UV−visible spectroscopy in some calcined samples and also by XRD in fewer cases, is not detected by XAS, except maybe in the case of the calcined 150 °C-dried sample, which contains the highest amount of ZnO. It is not surprising that ZnO is not clearly detected by XAS. Indeed, if one refers to the XRD patterns of mechanical mixtures of ZnO and silica, the amount of ZnO visible by XRD correspond to less than 10% of the zinc present in the calcined 150 °C-dried Zn/SiO_2 sample (Figure 8).

TABLE 3: ZnO Particle Size in Calcined Zn/SiO_2 Samples Dried at Various Temperatures, Measured from TEM Micrographs

	ZnO particle size			
	small		large	
drying T (°C)	average size (Å)	distribution (Å)	average size (Å)	distribution (Å)
90	28	15−44 (91p)		
120	29	15−59 (207p)	470	230−900 (21p)
150		112	32−843 (208p)	

d. Electron Microscopy. The TEM micrographs of the calcined 90 °C-dried Zn/SiO_2 sample show that the ZnO particles are small. In fact, these particles appear under the electron beam and might result from the reduction of the small amorphous ZnO particles. The average particle size was measured and found to be about 30 Å (Table 3). This result is consistent with the fact that the ZnO phase does not diffract but does exhibit a UV−visible absorption. In contrast, the calcined 120 and 150 °C-dried samples, whose ZnO is indicated by XRD (Figure 8), contain large ZnO particles, with a bimodal size distribution of particles for the first sample and only large particles (up to ∼900 Å) for the second (Table 3).

III. Discussion

1. Dried Zn/SiO_2 Samples. The XRD diffractograms of the 25 and 50 °C-dried Zn/SiO_2 samples indicate that the supported zinc phase is amorphous (Figure 3a). The DRIFT and XAS spectra of both samples lead to the conclusion that this amorphous phase is zinc nitrate (Figures 4b,c and 6).

When the samples are dried at higher temperature, i.e., between 90 and 150 °C, the XRD patterns (Figure 3) and the DRIFT spectra (Figure 4) show that zinc nitrate is transformed into hydroxynitrates: Zn_1 during drying at 90 or 120 °C and Zn_5 during drying at 150 °C. Zn_3, the third existing zinc hydroxynitrate, is not detected in our samples. As mentioned in the Introduction, the transformation of nitrate into hydroxynitrates at a temperature of ∼90 °C in silica-supported samples has already been observed in the case of Cu/SiO_2 samples prepared by impregnation with copper nitrate.[21]

The thermal decomposition of zinc nitrate and of the three zinc hydroxynitrates was extensively studied by Louër et al.[22,23,44] To summarize, they showed that $Zn(NO_3)_2 \cdot 6H_2O$ leads to Zn_1 at 65 °C. On the other hand, Zn_1 transforms into Zn_3 at 60−90 °C and then into ZnO at 160−190 °C, whereas Zn_5 transforms first into anhydric Zn_5 $[Zn_5(OH)_8(NO_3)_2]$ at temperatures lower than 100 °C, then into a mixture of ZnO and Zn_3 at 140 °C, and finally into ZnO at 190 °C.

The presence of the silica support seems to modify these transformations as Zn_3 is not detected after drying and ZnO is also not detected by either XRD or UV−visible spectroscopy when the sample is dried at 200 °C, i.e., above the temperature of decomposition of bulk zinc hydroxynitrates. In addition, the XAS study shows that, when zinc nitrate is supported on silica and dried at 120 and 150 °C, the presence of zinc hydroxynitrate (Zn_1 or Zn_5) could not be identified because the amount was too low, but Si and Zn atoms are present as second neighbors as in the case of the calcined samples. Furthermore, the XANES

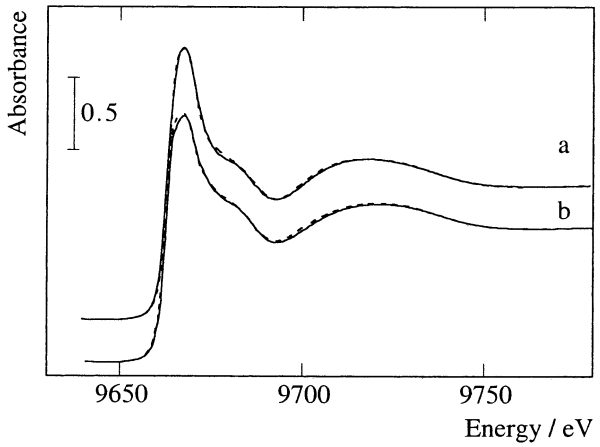

Figure 14. Comparison of the XANES spectra of (a) the 120 °C-dried sample with a linear combination of XANES spectra consiting of 65% of the calcined 120 °C-dried sample, i.e., of hemimorphite-type phase, and 35% of $[Zn(H_2O)_6]^{2+}$ and (b) the 200 °C-dried sample with a linear combination of XANES spectra consiting of 85% of calcined 200 °C-dried sample, i.e., of hemimorphite-type phase, and 15% of $[Zn(H_2O)_6]^{2+}$.

spectrum of the sample dried at 120 °C (Figure 6c) looks similar to those of the calcined samples (Figure 10a,b).

This is emphasized by the fact that the XANES spectrum of the 120 °C-dried sample fits well with the linear combination of 65% of the XANES spectrum of the calcined 120 °C-dried sample, i.e., 65% of a hemimorphite-type phase, and 35% of that of $[Zn(H_2O)_6]^{2+}$ (Figure 14a). This is also true for the XANES spectrum of the 200 °C-dried sample, which fits with a linear combination consisting of 85% of the XANES spectrum of the calcined 200 °C-dried sample and 15% of that of $[Zn(H_2O)_6]^{2+}$ (Figure 14b). Such fits could not be performed with the EXAFS signals because the EXAFS signal of $[Zn(H_2O)_6]^{2+}$ was recorded at RT whereas the others were recorded at 77 K. Hence, these XANES fits show that the Zn species in the 120 and 200 °C-dried samples is mainly a zinc silicate of hemimorphite type with a small amount of zinc nitrate.

It should be noted that it was useless to attempt to make linear combinations with the spectra of the zinc hydroxynitrates Zn_1 and Zn_5, because the references are too well-crystallized (long-range order) compared to the zinc species present in the samples. This is for the same reason that the XANES spectra of the calcined samples were used for the linear combinations for the 120 and 200 °C-dried samples, instead of that of the well-crystallized synthesized hemimorphite.

The formation of hemimorphite-type zinc silicate in the samples dried at temperatures above 90 °C indicates that the zinc species react with the silica surface during drying.

2. Calcined Zn/SiO_2 Samples. The XAS spectra of the 25, 50, and 200 °C-dried samples following calcination at 450 °C are similar. Their analysis shows that the zinc phase is a poorly crystallized zinc silicate of hemimorphite type.

Hence, for the 25 and 50 °C-dried samples, zinc nitrate is fully transformed into zinc silicate of hemimorphite type upon calcination as no ZnO is detected by XRD or UV−visible spectroscopy. Zinc nitrate is also almost fully transformed into this phase during drying at 200 °C (85%, see the preceding paragraph) and completely after further calcination treatment at 450 °C. The formation of ZnO is probably prevented because zinc nitrate is highly spread onto the silica surface in the wet state and also after drying at 25 and 50 °C because zinc nitrate remains amorphous. Hence, when these samples are calcined at 450 °C, i.e., heated at a temperature higher than that of decomposition of hydroxynitrates, zinc reacts with the silica surface and forms zinc silicate without forming ZnO.

It is well-known that zinc can easily react with silica to form silicate. This is the case when mixtures of ZnO and silica are heated at 900 °C, provided that the ZnO particles are small.[45] In this case, zinc silicate of willemite type, α-Zn_2SiO_4, forms.

When the samples are dried between 90 and 150 °C, although almost all of the zinc also forms a zinc silicate of hemimorphite type, the transformation of part of the zinc nitrate into hydroxynitrates during these drying steps leads to the formation of ZnO after calcination at 450 °C. This is consistent with the fact that bulk zinc hydroxynitrates transform into ZnO after decomposition at $T > 190$ °C.[22,23,44] The size of the ZnO particles depends on the drying temperature. The calcined 90 °C-dried Zn/SiO_2 sample, whose ZnO was detected by UV−visible spectroscopy only, shows small ZnO particles only (∼30 Å) in the TEM images, whereas the sample dried at 150 °C, which exhibits diffraction lines characteristic of ZnO after calcination, i.e., the largest amount of ZnO, contains large ZnO particles (>100 Å). This is also the only sample whose EXAFS results are slightly different from the others, probably because of the presence of ZnO.

Conclusion

The results and interpretations of this study are gathered in Table 4. It can be concluded from this work that incipient wetness impregnation of silica with a small volume of zinc nitrate solution leads to a film of zinc nitrate and, so to a highly spread zinc nitrate phase.

Depending on the temperature of drying, three types of Zn/SiO_2 samples are obtained: (i) After drying at 25 or 50 °C, the supported zinc phase is amorphous by XRD, but it was clearly identified as zinc nitrate by XAS and DRIFTS. (ii) When the samples are dried between 90 and 150 °C, part of the zinc nitrate transforms into zinc hydroxynitrate identified by XRD and DRIFTS: $Zn(OH)(NO_3)\cdot H_2O$ at 90 and 120 °C and $Zn_5(OH)_8(NO_3)_2\cdot 2H_2O$ at 150 °C. The other part that is amorphous was identified by XAS as a mixture of zinc nitrate (also observed by DRIFTS) and a zinc silicate phase of hemimorphite type [$Zn_4Si_2O_7(OH)\cdot H_2O$; ∼65% after drying at 120 °C]. This indicates that a rather large proportion of zinc reacts with the silica surface during the drying step at $T \sim 90$ °C. (iii) After being dried at 200 °C, the supported zinc phase is totally amorphous, and XAS shows that most of the zinc (∼85%) is of hemimorphite type, with the other part still being zinc nitrate (detected by DRIFTS).

After calcination, the Zn/SiO_2 samples that did not contain zinc hydroxynitrate after drying, i.e., the samples dried at 25, 50, and 200 °C, are amorphous (XRD). XAS shows that they contain only the zinc silicate phase of hemimorphite type. In contrast, the samples that contained zinc hydroxynitrate after drying, i.e., the samples dried at 90, 120, and 150 °C, also contain ZnO after calcination, but the size of the ZnO particles depends on the drying temperature. Drying at 150 °C leads to large ZnO particles (>100 Å according to TEM) after calcination that are detected by XRD. Drying at 90 °C leads to small ZnO particles (about 30 Å according to TEM) after calcination, detectable only by UV−visible spectroscopy. In both cases, XAS reveals that the main Zn species is still the silicate phase of hemimorphite type.

As mentioned in the Introduction, it is reported in the literature that calcination of Zn/SiO_2 samples prepared by impregnation with zinc nitrate leads to the formation of ZnO.[5,6,12] In most cases, zinc phase characterizations are not performed, but the

TABLE 4: Nature of the Various Zinc Species[a] in the Zn/SiO_2 Samples after Different Conditions of Drying and after Calcination

	after drying				after calcination at 450 °C				
drying *T* (°C)	XRD	DRIFTS	XAS	interpretation	XRD	UV−visible	mean particle size	XAS	interpretation
25	amorphous	$Zn(NO_3)_2$	$[Zn(H_2O)_6]^{2+}$	highly spread $Zn(NO_3)_2$	amorphous	no ZnO	−	hemimorphite	hemimorphite
50	amorphous	$Zn(NO_3)_2$	$[Zn(H_2O)_6]^{2+}$	highly spread $Zn(NO_3)_2$	amorphous	no ZnO	−	hemimorphite	hemimorphite
90	Zn_1	$Zn_1 + Zn(NO_3)_2$	−	hemimorphite? + Zn_1 and $Zn(NO_3)_2$	amorphous	ZnO	28 Å	hemimorphite	hemimorphite + small ZnO particles
120	Zn_1	−	hemimorphite (65%) + $[Zn(H_2O)_6]^{2+}$ (35%)	hemimorphite + traces of Zn_1 and $Zn(NO_3)_2$	ZnO (very weak)	ZnO	29 and 470 Å (bimodal)	hemimorphite	hemimorphite + ZnO particles
150	Zn_5	$Zn_5 + Zn(NO_3)_2$	−	hemimorphite? + Zn_5 and $Zn(NO_3)_2$	ZnO	ZnO	112 Å (very broad distribution)	hemimorphite + traces of another phase	hemimorphite + large ZnO particles
200	amorphous	ϵ [Zn_3 or Zn_5 + $Zn(NO_3)_2$]	hemimorphite (85%) + $[Zn(H_2O)_6]^{2+}$ (15%)	hemimorphite + traces of Zn_3 or Zn_5 and $Zn(NO_3)_2$	amorphous	no ZnO	−	hemimorphite	hemimorphite

[a] $Zn_1 = Zn(OH)(NO_3)\cdot H_2O$, $Zn_3 = Zn_3(OH)_4(NO_3)_2$, $Zn_5 = Zn_5(OH)_8(NO_3)_2\cdot 2H_2O$, hemimorphite = $Zn_4Si_2O_7(OH)_2\cdot H_2O$.

authors assume the formation of ZnO.[2,13] The present paper shows that ZnO cannot easily form on a silica support and that the main zinc phase is a poorly crystallized zinc silicate of hemimorphite type. This result is consistent with a very few studies that inferred the formation of zinc silicate whose nature had not been identified.[1,15] Moreover, this work demonstrates that the temperature of drying determines the final state of the material, i.e., the presence, or lack thereof, of ZnO as a minor phase.

Acknowledgment. We warmly thank Prof. Louër (University of Rennes) for helpful discussions, student E. Dran for the performance of additional experiments, and J. M. Krafft for his technical assistance in DRIFT spectroscopy. We also thank the technical staff of LURE synchrotron facility (Orsay, France).

Supporting Information Available: Table of fits using k^1 and k^3 data. Figures of EXAFS signals and of simulations of the two first shells of EXAFS signals. This material is available free of charge via the Internet at http://pubs.acs.org.

References and Notes

(1) Breuer, K.; Teles, J. H.; Demuth, D.; Hibst, H.; Schäfer, A.; Brode, S.; Domgörgen, H. *Angew. Chem., Int. Ed.* **1999**, *38*, 1401.
(2) Yoshida, H.; Murata, C.; Hattori, T. *J. Catal.* **2000**, *194*, 364.
(3) Shouro, D.; Moriya, Y.; Nakajima, T.; Mishima, S. *Appl. Catal. A: Gen.* **2000**, *198*, 275.
(4) Sagou, M.; Deguchi, T.; Nakamura, S. *Stud. Surf. Sci. Catal.* **1989**, *44*, 139.
(5) Rethwisch, D. G.; Dumesic, J. A. *J. Catal.* **1986**, *101*, 35.
(6) Ai, M. *Bull. Chem. Soc. Jpn.* **1991**, *64*, 1342.
(7) Poels, E. K.; Brands, D. S. *Appl. Catal. A: Gen.* **2000**, *191*, 83.
(8) van de Scheur, F. T.; Staal, L. H. *Appl. Catal. A: Gen.* **1994**, *108*, 63.
(9) Shiau, C.; Chen, S.; Tsai, J. C.; Lin, S. I. *Appl. Catal. A: Gen.* **2000**, *198*, 95.
(10) Millar, G. J.; Rochester, C. H.; Bailey, S.; Waugh, K. C. *J. Chem. Soc., Faraday Trans.* **1993**, *89*, 1109.
(11) Burch, R.; Chappell, R. J.; Golunski, S. E. *J. Chem. Soc., Faraday Trans. 1* **1989**, *85*, 3569.
(12) Naito, S.; Tanimoto, M.; Soma, M. *J. Chem. Soc., Chem. Commun.* **1992**, 1443.
(13) Zhao, B.; Wu, N.; Gui, L.; Zhang, L.; Bai, J.; Xie, Y.; Tang, Y. *Sci. Sin.* **1986**, *29*, 579.
(14) Yao, B.; Shi, H.; Bi, H.; Zhang, L. *J. Phys.: Condens. Matter.* **2000**, *12*, 6265.
(15) Guo, Q.; Gui, L.; Huang, H.; Zhao, B.; Tang, Y. *J. Catal.* **1990**, *122*, 457.
(16) Che, M.; Cheng, Z. X.; Louis, C. *J. Am. Chem. Soc.* **1995**, *117*, 2008.
(17) Burattin, P.; Che, M.; Louis, C. *J. Phys. Chem. B* **1997**, *101*, 7060.
(18) Clause, O.; Kermarec, M.; Bonneviot, L.; Villain, F.; Che, M. *J. Am. Chem. Soc.* **1992**, *114*, 4709.
(19) Toupance, T.; Kermarec, M.; Lambert, J.-F.; Louis, C. *J. Phys. Chem. B* **2002**, *106*, 2277.
(20) Trujillano, R.; Villain, F.; Lambert, J.-F.; Louis, C., manuscript in preparation.
(21) Toupance, T.; Kermarec, M.; Louis, C. *J. Phys. Chem. B* **2000**, *104*, 965.
(22) Louër, D.; Gaudin-Louër, M.; Weigel, D. *C. R. Acad. Sci.* **1968**, *266C*, 59.
(23) Louër, M.; Louër, D.; Weigel, D. *C. R. Acad. Sci.* **1970**, *270C*, 881.
(24) Stählin, W.; Oswald, H. R. *J. Solid State Chem.* **1971**, *3*, 252
(25) Hermans, L. A. M.; Geus, J. W. In *Preparation of Catalysts II*; Delmon, B., Grange, P., Jacobs, P. A., Poncelet, G., Eds.; Elsevier: Amsterdam, 1979; p 113.
(26) Catillon, S.; Peltre, M.-J.; Lauron-Pernot, H.; Louis, C., manuscript to be published.
(27) Michalowicz, A. EXAFS pour le MAC, Logiciels pour la Chimie. *Soc. Fr. Chim., Paris* **1991**, 102.
(28) Lengeler, B.; Eisenberger, P. *Phys. Rev. B* **1980**, *21*, 4507.
(29) James, F.; Roos, M. *MINUIT*: CERNID Internal Report 75/20; Program Library, CERN Computing Center, CERN: Geneva, Switzerland, 1976.

(30) (a) Rehr, J. J.; Mustre de Leon, J.; Zabinsky, S. I.; Albers, R. C. *J. Am. Chem. Soc.* **1991**, *113*, 5135. (b) Mustre de Leon, J.; Rehr, J. J.; Zabinsky, S. I.; Albers, R. C. *Phys. Rev. B* **1991**, *44*, 4146.

(31) Faust, G. T. *Am. Miner*. **1951**, *36*, 795.

(32) Roy, D. M.; Mumpton, F. A. *Econ. Geol.* **1956**, *51*, 432.

(33) Mondésir, H.; Decarreau, A. *Bull. Minéral.* **1987**, *110*, 409.

(34) Decarreau, A.; Mondésir, H.; Besson, G. *C. R. Acad. Sci. Paris (Sér. II)* **1989**, *308*, 301.

(35) Chouillet, C.; Krafft, J.-M.; Louis, C.; Lauron-Pernot, H. *Spectrochim. Acta A*, submitted.

(36) Gatehouse, B. M.; Livingstone, S. E.; Nyholm, R. S. *J. Chem. Soc*. **1957**, 4222.

(37) Addison, C. C.; Sutton, D. In *Progress in Inorganic Chemistry*; Cotton, F. A. Ed.; Interscience Publishers: New York, 1967; Vol. 8, p 201.

(38) *Encyclopedia of Inorganic Chemistry*; King, R. B., Ed.; John Wiley: New York, 1994; Vol. 7, p 3728.

(39) Carriat, J. Y.; Che, M.; Kermarec, M.; Verdaguer, M.; Michalowicz, A. *J. Am. Chem. Soc*. **1998**, *120*, 2059.

(40) Abrahams, S. C.; Bernstein, J. L. *Acta Crystallogr*. **1969**, *B25*, 1233.

(41) (a) McDonald, W. S.; Cruickshank, D. W. J. *Z. Kristallogr*. **1967**, *124*, 180. (b) Libowizky, E.; Kohler, T.; Armbruster, T.; Rossmann, G. R. *Eur. J. Mineral.* **1997**, *9*, 903.

(42) (a) Simonov, M. A.; Sandomirskii, P. A.; Egorov-Tismenko, Y. K.; Belov, N. V. *Sov. Phys. Dokl.* **1977**, *22*, 622. (b) Simonov, M. A.; Belov, N. V. *Moscow Univ. Geol. Bull.* **1978**, *33*, 43.

(43) Rayner, J. H.; Brown, G. *Clay Miner.* **1973**, *21*, 103.

(44) Auffredic, J.-P.; Louër, D. *J. Solid State Chem*. **1983,** *46*, 245.

(45) Suzuki, H.; Yasuoka, S.; Rissen, Y.; Nakabayashi, H. *Gakujutsu Kiyo-Kochi Kogyo Koto Semmon Gakko* **1988**, *29*, 39.